Pinning-Based Switching Control of Cyber-Physical Supercapacitor Energy Storage Systems

Heng Li, *Member, IEEE*, Jun Peng, *Member, IEEE*, Jianping He, *Member, IEEE*, Zhiwu Huang, *Member, IEEE*, Jing Wang, *Senior Member, IEEE*, Liang He, *Senior Member, IEEE*, and Jianping Pan, *Senior Member, IEEE*

***Abstract*— This paper presents a pinning-based switching control approach for the charging and cell balancing of supercapacitors. The developed supercapacitor energy storage system is modeled as a cyber-physical system (CPS), which consists of a physical layer, a cyber layer, and a control layer. In the physical layer, the switched resistor circuit is employed to charge and balance supercapacitor cells, and the physical system is mathematically characterized using the switched systems' theory. The cyber layer is modeled with the graph theory to characterize the accessibility of the reference voltage and the availability of neighbors' information to cells. In the control layer, a pinning-based switching control law is proposed to balance cell voltages during the charging process. The stability of the CPS is rigorously proved and the closed-loop model of the CPS is derived using the block diagram. A laboratory testbed has been built to verify the effectiveness of the proposed method. Extensive experiment results show that the proposed pinning control method can reduce the voltage deviation and improve the energy efficiency when compared with the classical decentralized control method. Some practical issues about the implementation of the proposed method are also discussed.**

***Index Terms*— Cyber-physical systems (CPSs), energy storage systems, pinning control, supercapacitors.**

Manuscript received November 18, 2018; revised February 15, 2019; accepted May 2, 2019. Manuscript received in final form May 4, 2019. This work was supported in part by the National Natural Science Foundation under Grant 61803394, Grant 61672537, Grant 61773257, and Grant 61772558, in part by the Hunan Provincial Natural Science Foundation of China under Grant 2019JJ50822, in part by the NSF under Grant CNS-1739577, and in part by the Natural Sciences and Engineering Research Council (NSERC). Recommended by Associate Editor W. Zhang. *(Corresponding author: Zhiwu Huang.)*

H. Li and J. Peng are with the School of Computer Science and Engineering, Central South University, Changsha 410083, China (e-mail: liheng@csu.edu.cn; pengj@csu.edu.cn).

J. He is with the Department of Automation, Shanghai Jiao Tong University, Shanghai 200240, China, and also with the Key Laboratory of System Control and Information Processing, Shanghai Jiao Tong University, Shanghai 200240, China (e-mail: jphe@sjtu.edu.cn).

Z. Huang is with the School of Automation, Central South University, Changsha 410083, China (e-mail: hzw@csu.edu.cn).

J. Wang is with the Electrical and Computer Engineering Department, Bradley University, Peoria, IL 61625 USA (e-mail: jingwang@bradley.edu).

L. He is with the Department of Computer Science and Engineering, University of Colorado Denver, Denver, CO 80124 USA (e-mail: liang.he@ucdenver.edu).

J. Pan is with the Department of Computer Science, University of Victoria, Victoria, BC V8W3P6, Canada (e-mail: pan@uvic.ca).

Color versions of one or more of the figures in this paper are available online at http://ieeexplore.ieee.org.

Digital Object Identifier 10.1109/TCST.2019.2916039

I. Introduction

RECENT years have seen a growing interest in the deployment of supercapacitors in promising applications, including public transportation [1]–[3], hybrid energy storage systems [4]–[6], and portable electronics [7]–[9], due to their superiorities over conventional batteries in certain aspects, such as high power density, low series-equivalent-resistance (ESR), and extremely long lifetime [10]–[13].

In practical applications, supercapacitor cells are typically connected in series as a fixed module to meet the voltage requirement of the application scenarios [14]. Due to the manufacturing tolerance, cells typically suffer from voltage imbalance, which may lead to the overcharging of some cells during the charging process, resulting in the reliability and lifetime degradations of the system. Thus, cell-balancing circuits are typically applied in energy storage systems to eliminate the imbalance and improve the system reliability.

Existing cell-balancing circuits can be summarized into two categories, i.e., active balancing circuits and passive balancing circuits [15]. The active balancing circuits transfer the energy from high-voltage cells to low-voltage ones through active components, e.g., capacitors, inductors, or dc–dc converters. The active circuits benefit from high energy efficiency, while the size of the balancing circuit is large and the cost is relatively high [14]. In passive balancing circuits, passive components, e.g., resistors, are utilized to dissipate the excessive energy of the high-voltage cells. Although the energy efficiency is relatively low, the passive balancing circuits are widely used in applications, where the system size and cost budget are limited, especially in low-power applications [16]. Specifically, the switched resistor circuit has been a popular balancing circuit in practice due to its good tradeoff between the performance and cost [16]–[18].

Fig. 1 shows the schematic of the switched resistor circuit in an n-cell supercapacitor energy storage system, where each cell is connected in parallel with a balancing resistor through a switch. For the switched resistor circuit, the primary task is to prevent cells from overcharging during the charging process [14]. Thus, effective cell-balancing charging control methods are necessary for the circuit.

A classical cell-balancing charging method for the switched resistor circuit is the decentralized control approach [14]–[17],

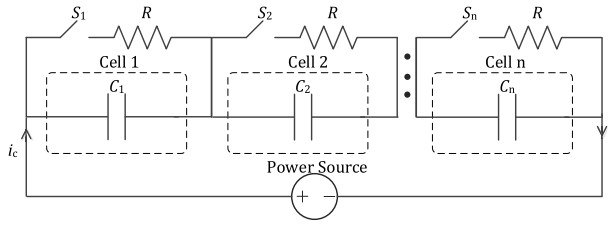

Fig. 1. Switched resistor circuit for an n-cell supercapacitor energy storage system.

where the ON/OFF status of a switch is determined by comparing the corresponding cell's voltage with the reference voltage. If the cell voltage is above the reference, the switch will be ON; then the charging current is expected to be shunted to the balancing resistor and the cell voltage is stabilized toward the reference voltage [16]. Although the decentralized control method has been widely used in practice, there are two limitations of the method: 1) cells are easily overcharged due to the voltage deviation effect caused by the thermal heating of balancing resistors and 2) the energy efficiency is relatively low due to the high-voltage profiles of cells during the charging process.

In a high-level pinning control theory, cells in the energy storage system can be regarded as nodes in the graph, and the reference voltage can be viewed as the pinner. Pinning control is a feedback control strategy for the synchronization and consensus of complex dynamical networks, where a virtual leader (pinner) directly controls a fraction of nodes (pinned nodes), while the other nodes track the pinner through the interaction networks with the pinned nodes [19]. From this observation, the decentralized control method is a special case of the pinning control, where the pinner directly interacts with all nodes. It is of practical significance to generalize the decentralized control to a more systematic pinning control for charging supercapacitors, and further explore whether the voltage deviation effect can be alleviated and the energy efficiency can be improved, which motivates the work in this paper.

In this paper, we propose a pinning-based switching control method to charge and balance supercapacitors simultaneously. In the proposed method, the ON/OFF status of a switch is determined by comparing the corresponding cell's voltage with both the reference voltage and those of its neighbors. As the dynamics of each cell have two modes depending on the ON/OFF of the switch, a switching law is proposed to stabilize the physical system, and the stability of the closed-loop system is analyzed with the switched systems' theory. Switched systems are a class of hybrid systems, which consists of a family of dynamic subsystems along with a switching law governing the switching among them [20]–[22]. Switched systems can be efficiently used to model many practical systems that are inherently multimodal, i.e., several dynamical subsystem models are required to describe their behaviors [21].

The main contributions and approaches of this paper are summarized as follows.

1) A cyber-physical system (CPS) framework is developed for the modeling, controller design, and performance analysis of the supercapacitor energy storage systems.
2) A pinning-based switching control method is proposed to charge and balance supercapacitor cells. The stability of the CPS is rigorously proved and the closed-loop model of the CPS is derived using the block diagram.
3) A laboratory testbed is built and the experimental results indicate that the voltage deviation is alleviated and the energy efficiency is improved when compared with the decentralized control method.

The remainder of this paper is organized as follows. Section II reviews the related work. The preliminaries and system modeling are presented in Section III. The proposed method is introduced in Section IV. We evaluate the performance of the proposed method with experiment results in Section V. This paper is concluded in Section VI.

II. Related Work

The pinning control is typically referred to as the *leader–follower consensus* in the literature, where the leader represents the reference information specified by the designer. Another closely related protocol is the *leaderless consensus*, where all nodes are driven to an unprescribed common value [23]. The leader–follower consensus is reduced to the leaderless one when the pinning matrix from the leader to the followers is a zero matrix. Both consensus protocols have been widely used in designing distributed energy systems [24]–[29].

Manaffam *et al.* [24] proposed a pinning control method for the voltage synchronization of microgrids. The lower and upper bounds on the algebraic connectivity of the network with respect to the reference are derived. Yan *et al.* [25] proposed an energy-aware leader–follower tracking control for electric-powered multiagent systems, where the energy of each agent is assumed to be limited. The proposed leader–follower consensus is established in a model predictive control (MPC) framework to maximize the operation range of agents. In [26], a pinning-based current synchronization method is proposed for multiple charging modules, where the output current of each module tracks both the reference current and the currents of its neighbors.

In [27], a leaderless consensus-based state-of-charge (SoC) balancing method is proposed for Lithium-Ion batteries with the cell-to-cell equalizing topology. A combinatorial 0–1 optimization problem is formulated and solved to optimally choose added equalizers that lead to the minimal balancing time. In [28], a distributed cell-balancing method is proposed for supercapacitors using the leaderless consensus protocol. The performance of the cell-balancing system is verified with different balancing resistances. Wang *et al.* [29] studied the controllability and observability of a networked battery system with bypassing balancing circuits. A switching algorithm is designed to achieve the SoC balancing of batteries using a leaderless consensus protocol.

Motivated by these works, in this paper, we propose a pinning-based switching control method for the charging and cell balancing of supercapacitors. We experimentally compare the proposed pinning-based cell-balancing method with existing leaderless-consensus ones [27]–[29], and the experiment results show that while the leaderless consensus protocols significantly prolong the charging time, the proposed method

can synchronize cell voltages without prolonging the charging time.

III. Preliminaries and System Modeling

In this section, we first introduce the preliminary knowledge about switched systems. Then, we model the supercapacitor energy storage system using the switched systems' theory and the graph theory.

A. Switched Systems

A switched system consists of a collection of indexed differential equations and a switching signal governing the switching among them [30]. Specifically, a switched linear system can be mathematically modeled as [31]

$$\dot{x} = A^{\sigma} x + B^{\sigma} u \tag{1}$$

where x and u are the system state and the control input, respectively, σ is a piecewise constant, called the switching signal, which takes its values in the finite set $S = \{1, 2, \cdots, M\}$ with M being the number of subsystems, and A^{σ} and B^{σ} are the state and input matrices of the σth subsystem, respectively.

The design task for the switched system (1) is to find switching signal σ and control input u to stabilize the closed-loop system [32]. For the case where the control input is absent or given in advance, and $M = 2$, i.e., there are only two subsystems, we have Lemma 1 to evaluate whether the switched system can be stabilized with a sequence of switching signals.

Lemma 1 [33]–[35]: There exists a switching sequence $\sigma(t)$ such that the switched system (1) is quadratically stable if and only if there exists $\alpha \in [0, 1]$ such that

$$A_{\text{eq}} = \alpha A^1 + (1 - \alpha) A^2 \tag{2}$$

is negative definite, i.e., the eigenvalues of A_{eq} lie in the open left-half complex plane.

Lemma 1 will be used to examine whether the supercapacitor charging system can be stabilized with a switching sequence.

B. System Modeling

1) Physical Modeling: As shown in Fig. 1, each cell in the physical system is connected in parallel with a balancing resistor R through a switch S_k. The ESRs of supercapacitors account for the voltage drop effect when the cell balancing is finished and the charging current is terminated [13]. As the ESRs of supercapacitors are relatively small (e.g., m Ω level), cells can be simplified as a capacitor in the cell-balancing design [14], [16]. Then, the voltage dynamics of each cell are derived as

$$\dot{v}_k = \frac{i_c}{C_k} - \frac{v_k}{RC_k} s_k, \quad k = 1, \ldots, n \tag{3}$$

where C_k, v_k, and s_k represent the capacitance, voltage, and duty cycle of cell k, respectively, R is the resistance of the balancing resistor, and i_c is the charging current from the external power source.

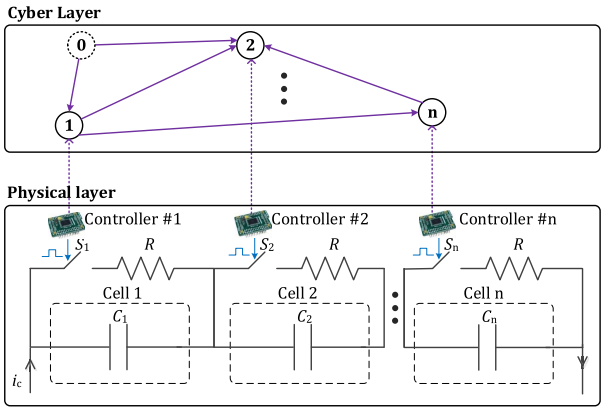

Fig. 2. Cyber-physical modeling of the supercapacitor energy storage system.

The external power source is chosen as a constant-current (CC) source, which implies that the charging current i_c is a constant. Conventional batteries are typically charged by a constant-current constant-voltage (CC-CV) source, where the CV stage decreases the charging current and eliminates the voltage drops on ESRs. Since the ESR of supercapacitors is much smaller, supercapacitors are typically charged with a CC source [12].

The differential $\dot{v}_k$ is called the charging rate of cell k, which indicates the voltage increase rate of the cell during the charging process. Based on the ON/OFF status of switch k, the charging rate of cell k is derived as

$$\begin{cases} \dot{v}_k = \dfrac{i_c}{C_k}, & s_k = 0 \\ \dot{v}_k = \dfrac{i_c}{C_k} - \dfrac{v_k}{RC_k}, & s_k = 1 \end{cases} \tag{4}$$

where we find that when the switch k is OFF, i.e., $s_k = 0$, cell k is charged with the highest charging rate; while when switch k is ON, i.e., $s_k = 1$, the charging rate of cell k decreases with cell voltage v_k. Specifically, the charging rate decreases to zero when $v_k = i_c R$. Thus, we commonly choose $v_0 = i_c R$ as the reference voltage for cells.

It is shown in (4) that the voltage dynamics of cell k have two subsystems based on the switching of duty cycle s_k. Thus, the system (4) can be modeled as a switched system

$$\dot{x}_k = A_k^{\sigma_k} x_k + B_k u, \quad k = 1, \ldots, n \tag{5}$$

where the system state $x_k = v_k$, the control input $u = i_c$, the switching signal $\sigma_k = s_k + 1 \in \{1, 2\}$, and the system parameters are defined as

$$A_k^1 = 0, \quad A_k^2 = -\frac{1}{RC_k}, \quad B_k = \frac{1}{C_k}. \tag{6}$$

Now, we have built the physical model of each cell using the switched systems' theory. In what follows, we will model the communication interaction among cells using the graph theory.

2) Cyber Modeling: The cyber-physical modeling of the supercapacitor energy storage system is shown in Fig. 2, where each cell in the physical layer is mapped to a node in the cyber layer. Specifically, node 0 is a virtual node that represents the

reference for cells and does not correspond to any cell in the physical layer.

The interactions among cells can be modeled as a directed graph (υ, ε), where the node set υ represents the cells in the physical layer, and the edge set ε represents the communication links among cells. The edge direction specifies the information flow between cells. If there is a directed link from cell m to cell k, i.e., cell k can receive information from cell m, node m is called a neighbor of node k. The neighbor set of node k is denoted as N_k, where the number of node k's neighbors is denoted as d_k, which is also called the in-degree of node k [36]. The in-degree matrix is a diagonal matrix defined as $\mathbf{D} = \text{diag}(d_k)_n$. The adjacency matrix is defined as $\mathbf{A} = [a_{km}]_{n\times n}$ with $a_{km} = 1$ if there is a link from node m to node k and $a_{km} = 0$ otherwise. Then, the Laplacian matrix of the graph is defined as $\mathbf{L} = \mathbf{D} - \mathbf{A}$. The interactions among the virtual node 0 and the other nodes are represented by the diagonal pinning matrix $\mathbf{G} = \text{diag}(g_k)_n$ with $g_k = 1$ if node 0 pins to node k directly, and $g_k = 0$ otherwise.

The interactions of the cells in the supercapacitor energy storage system can be systematically characterized by the two graph matrices $\mathbf{L}$ and $\mathbf{G}$. Specifically, the Laplacian matrix $\mathbf{L}$ represents the availability of the neighbors' information to cells and the pinning matrix $\mathbf{G}$ characterizes the accessibility of the reference information to cells.

IV. Pinning-Based Switching Control

In this section, we propose a pinning-based switching control strategy for the supercapacitor charging system. We first show some properties about the system to be used in the stability analysis. Then, a pinning control method is proposed, where the stability and convergence are rigorously proved. The closed-loop model is derived using the block diagram. Several performance metrics are introduced to evaluate the performance of the proposed charging method.

A. System Properties

We introduce some properties about the physical system characterized by (5) and (6) that can be utilized in the charging controller design and stability analysis. By examining the dynamics of the switched system, we find that the second subsystem is stable as A_k^2 is negative definite in (6). Then, the closed-loop system can be guaranteed stable by setting $\sigma_k = 2$. These observations are summarized in Lemmas 2 and 3.

Lemma 2: There exists a switching sequence $\sigma_k(t)$ such that the switched system characterized by (5) and (6) is quadratically stable.

Proof: From (6), we know that $A_k^2 < 0$. Then, for any $\alpha \in [0, 1)$, we have $A_{\text{eq}} = (1-\alpha)A_k^2 < 0$. Based on Lemma 1, we know that there exists a switching sequence $\sigma_k(t)$ such that the switched system characterized by (5) and (6) is quadratically stable. □

Lemma 2 shows that the cell-balancing charging system can be stabilized by at least one switching sequence. We now need to determine a specific switching sequence to do that. As it is known that the switching signal $\sigma_k = 2$ can stabilize the closed-loop system, the problem is when to trigger $\sigma_k = 2$ in the charging process. The design task for the cell-balancing charging is to ensure that the voltages of cells are stabilized at the reference voltage x_0. When $x_k < x_0$, from (4), we find that the switching signal σ_k can be 1 (i.e., fast charging) or 2 (i.e., slow charging). However, when $x_k \geq x_0$, the switching signal σ_k has to be 2, otherwise cells are overcharged and the closed-loop system cannot be stabilized. Then, we have Lemma 3.

Lemma 3: The switched system characterized by (5) and (6) for any cell k can be stabilized, and cell voltage x_k converges to $x_0 = i_c R$ asymptotically in the charging process if the switching sequence is chosen as

$$\sigma_k(t) = 2 \quad \forall x_k(t) \geq x_0. \tag{7}$$

Proof: When $\sigma_k(t) = 2$, we have $A_k^2 = -(1)/(\text{RC}_k) < 0$, which means that the closed-loop system is asymptotically stable. From (4), we can find that the only equilibrium for cell k is $x_k = x_0$. Thus, if we set $\sigma_k(t) = 2$ when $x_k(t) \geq x_0$, the closed-loop system is stable and the state x_k converges to x_0 asymptotically. □

The condition (7) is sufficient but not necessary for the system's stability and convergence in the charging process. For instance, if we first set $\sigma_k(t) = 1$ and then set $\sigma_k(t) = 2$ when $x_k(t) \geq x_0$, the closed-loop system can still be stable as long as $\sigma_k(t) = 2$ is the final stage. However, setting $\sigma_k = 1$ when a cell is fully charged results in the overcharging of the cell, which should be avoided in practical systems. Lemma 3 is useful in proving the stability of the proposed pinning control method, which will be illustrated in what follows.

B. Pinning Control

For the supercapacitor charging system with n cells, the classical decentralized control signal is extensively used in practical applications, where the signal is chosen as the negative feedback between the reference and the voltage of each cell. In this section, we propose a pinning-based switching control signal for the supercapacitor charging system by considering both the accessibility of the reference and the availability of the neighbors' information to cells. It will be shown later that the existing switching signals are a special case of the proposed design. Specifically, the switching signal σ_k for cell k is designed as

$$\sigma_k = \text{sign}(\delta_k) \tag{8}$$

where the switching logic $\text{sign}(\cdot)$ is defined as

$$\text{sign}(\delta_k) = \begin{cases} 2, & \forall \delta_k \leq 0 \\ 1, & \text{otherwise} \end{cases} \tag{9}$$

and the tracking error δ_k is designed as

$$\delta_k = g_k(x_0 - x_k) + \sum_{m\in N_k} a_{km}(x_m - x_k) \tag{10}$$

where x_0 is the reference voltage, x_k is the voltage of cell k, x_m values are the voltages of neighbors of cell k, and g_k and a_{km} are the pinning and adjacent elements, respectively. For the vector arguments, the switching logic $\text{sign}(\cdot)$ is defined

componentwise. Thus, the treatments are similar for the vector and scalar states.

The tracking protocol (10) is a pinning control method, which characterizes all the possible interactions between the reference and cells, as well as those among cells [19]. The first term of the tracking protocol (10) characterizes the accessibility of the reference to cells. If the reference pins to cell k, $g_k = 1$; otherwise $g_k = 0$. The second term describes the availability of the neighbors' information to cells. If cell k can receive information from cell m, $a_{km} = 1$; otherwise, $a_{km} = 0$. If $a_{km} = 0$ and $g_k = 1$ for any $k, m \in \upsilon$, the switching signal (8)–(10) reduces to the classical decentralized control, i.e., each cell makes the control decision based on the comparison between the reference and its own voltage. If $x_k < x_0$, we have $\sigma_k = 1$, i.e., $s_k = 0$. Then, from (4), we know that cell k is charged with a high charging rate. If $x_k \geq x_0$, we have $\sigma_k = 2$, i.e., $s_k = 1$. Then, from Lemma 3, we know that the cell voltage will be stabilized to $x_0 = i_c R$. If $g_k = 0$ and there exists $k, m \in \upsilon$ that $a_{km} = 1$, the switching signal reduces to a leaderless consensus control. If $x_k < x_m$, we have $\sigma_k = 1$, i.e., $s_k = 0$, implying that cell k is charged faster than cell m; otherwise, we have $\sigma_k = 2$, i.e., $s_k = 1$, implying that cell k is charged slower than cell m. Such a regulation mechanism will lead to the voltage synchronization of cells during the charging process.

From the above analysis, we can find that: 1) the first term of (10) stabilizes the cell voltage to the reference x_0 when a cell is fully charged and 2) the second term of (10) synchronizes the cell voltage with its neighbors during the charging process. Specifically, the first term is characterized by the pinning matrix $\mathbf{G}$ and the second term is characterized by the Laplacian matrix $\mathbf{L}$.

In the charging process, the voltages of cells are expected to increase to the reference voltage x_0. When $x_k(t) < x_0$, cells are charged by the proposed method, where the voltages are increasing toward the reference voltage. The stability and the convergence $x_k \to x_0$ can be evaluated by examining if $\sigma_k(t) = 2$ when $x_k(t) \geq x_0$ for any $k \in \upsilon$, as shown in Lemma 3. Then, we have Theorem 1.

Theorem 1: Consider the supercapacitor charging system shown in Fig. 1, where the dynamics of each cell are characterized by (5) and (6). The closed-loop system can be stabilized by switching law (8)–(10) and cell voltages converge to the reference voltage x_0 asymptotically in the charging process if either of the following two cases holds.

1) *Case A:* The reference pins to all cells.
2) *Case B:* The reference pins to at least one cell, and there is a directed spanning tree among cells, where the pinned cell is the root of the tree.

Proof: Define the collective vector form of state $\mathbf{X}$, reference $\mathbf{X_0}$, tracking error Δ, and switching signal $\boldsymbol{\sigma}$, respectively, by

$$\begin{aligned} \mathbf{X} &= [\, x_1 \quad x_2 \quad \cdots \quad x_n \,]^T \\ \mathbf{X}_0 &= [\, x_0 \quad x_0 \quad \cdots \quad x_0 \,]^T \\ \Delta &= [\, \delta_1 \quad \delta_2 \quad \cdots \quad \delta_n \,]^T \\ \boldsymbol{\sigma} &= [\, \sigma_1 \quad \sigma_2 \quad \cdots \quad \sigma_n \,]^T. \end{aligned} \tag{11}$$

From (10), we have

$$\begin{aligned} \delta_k &= g_k x_0 - g_k x_k + \sum_{m \in N_k} a_{km} x_m - \sum_{m \in N_k} a_{km} x_k \\ &= -(d_k + g_k) x_k + g_k x_0 + \sum_{m \in N_k} a_{km} x_m. \end{aligned} \tag{12}$$

The tracking error (12) is written in the matrix-vector form as

$$\begin{aligned} \Delta &= -(\mathbf{D} + \mathbf{G})\mathbf{X} + \mathbf{G}\mathbf{X}_0 + \mathbf{A}\mathbf{X} \\ &= -(\mathbf{D} - \mathbf{A})\mathbf{X} + \mathbf{G}(\mathbf{X}_0 - \mathbf{X}) \\ &= -\mathbf{L}\mathbf{X} + \mathbf{G}(\mathbf{X}_0 - \mathbf{X}). \end{aligned} \tag{13}$$

Note that the row sum of the Laplacian matrix is zero, then we have $\mathbf{L}\mathbf{X}_0 = \mathbf{0}$, where $\mathbf{0}$ is a vector with all zero elements. Substituting it to (13) yields

$$\Delta = \mathbf{L}\mathbf{X}_0 - \mathbf{L}\mathbf{X} + \mathbf{G}(\mathbf{X}_0 - \mathbf{X}) = (\mathbf{L} + \mathbf{G})(\mathbf{X}_0 - \mathbf{X}). \tag{14}$$

We first prove that Case A can stabilize the closed-loop system. When the reference pins to all cells, $\mathbf{L} = \mathbf{0}_{n \times n}$ is a zero matrix and $\mathbf{G} = \mathbf{I}_{n \times n}$ is an identity matrix. Then, from (14), we have

$$\Delta \leq \mathbf{0} \Rightarrow \mathbf{X}_0 - \mathbf{X} \leq \mathbf{0}. \tag{15}$$

Following the switching logic in (9), we have:

$$\boldsymbol{\sigma} = \mathbf{2}, \quad \mathbf{X} \geq \mathbf{X}_0. \tag{16}$$

Equation (16) implies that when $x_k(t) \geq x_0$ for all cells, we have $\sigma_k = 2$, $\forall k \in \upsilon$. Then, based on Lemma 3, we know that the closed-loop system is stable and the voltage $\mathbf{X}$ converges to the reference voltage $\mathbf{X}_0$ asymptotically.

Now, we prove that Case B can also stabilize the closed-loop system. When the reference pins to at least one cell, and there is a directed tree among all cells, where the pinned cell is the root, the matrix $\mathbf{L} + \mathbf{G}$ is positive definite and thus invertible [19]. Thus, from (14), we have

$$\Delta \leq \mathbf{0} \Rightarrow \mathbf{X}_0 - \mathbf{X} \leq (\mathbf{L} + \mathbf{G})^{-1}\mathbf{0} \Rightarrow \mathbf{X}_0 - \mathbf{X} \leq \mathbf{0}. \tag{17}$$

Then, based on (16) and Lemma 3, we know that the closed-loop system is stable and the voltage $\mathbf{X}$ converges to the desired voltage $\mathbf{X}_0$ asymptotically. This completes the proof. □

From the above analysis, we know that the proposed pinning-based switching control method can achieve the voltage stabilization and voltage synchronization in the charging process by appropriately choosing the communication topology among cells. The stability and convergence of the proposed design have been rigorously proved in Theorem 1. In what follows, we derive the collective model of the closed-loop system.

C. Closed-Loop Modeling

In order to evaluate the performance of the closed-loop system, we need to develop the closed-loop model of the supercapacitor energy storage system. The MIMO model of the switched system (5) is represented as

$$\dot{\mathbf{X}} = \mathbf{A}^{\boldsymbol{\sigma}}\mathbf{X} + \mathbf{B}u \tag{18}$$

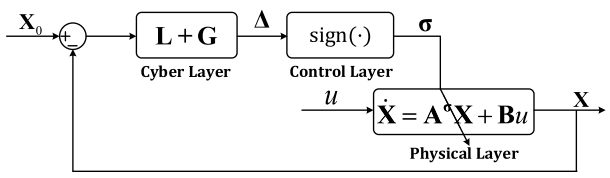

Fig. 3. Cyber-physical framework of the closed-loop system.

where $\mathbf{A}^{\boldsymbol{\sigma}} = \text{diag}(A_k^{\sigma_k})_n$ and $\mathbf{B} = \text{diag}(B_k)_n$ are the state and input matrices of the collective system, respectively.

We derive the closed-loop model of the supercapacitor energy storage system using block diagrams, where signals represent the variables of the system and blocks represent the models of the corresponding layer. The input vector of the closed-loop system is $\mathbf{X}_0$, and the output vector of the system is $\mathbf{X}$. From (14), it is observed that the negative feedback vector $\mathbf{X}_0 - \mathbf{X}$ is input to the cyber-layer model $\mathbf{L}+\mathbf{G}$ to generate the tracking error vector Δ. Then, the tracking error vector Δ is injected to the control-layer model (8) to generate the switching control vector $\boldsymbol{\sigma}$. Finally, the switching control vector $\boldsymbol{\sigma}$ is injected to the physical-layer model (18) to supply the output voltage $\mathbf{X}$. Another input of the physical layer is u, i.e., the charging current from the external power source. By connecting the above layers according to the signal flow, the cyber-physical framework of the closed-loop control system is developed in Fig. 3, where we find that the developed closed-loop system model consists of three layers [37], i.e., a physical layer, a cyber layer, and a control layer.

In the closed-loop model of the CPS, the physical layer (18) and the control layer (8) are predefined. This implies that the performance of the CPS will be determined by the cyber-layer model $\mathbf{L}+\mathbf{G}$. It will be shown later that different communication topologies have significant influence on the performance of the CPS. In order to evaluate the performance of the CPS under different communication topologies, we first introduce several performance metrics that will be used in the performance evaluation.

D. Performance Metrics

The performance of the CPS will be evaluated in the following aspects, i.e., charging time, energy efficiency, and voltage deviation.

1) Charging Time: Charging time is an important metric that affects the user satisfaction in many applications. In the proposed cell-balancing charging scheme, the charging and the cell balancing are conducted for cells simultaneously. A reasonable requirement is that the cell balancing should not prolong the charging time. In this paper, the charging time for the supercapacitor energy storage system is defined as the time that the last cell is fully charged. We will compare the charging time of the proposed method with those of the decentralized control method and the leaderless consensus method experimentally.

2) Energy Efficiency: Energy efficiency is another metric to evaluate the performance of the cell-balancing charging system. The energy efficiency of the supercapacitor charging system is defined as the ratio of the energy stored in the supercapacitors to the input energy from the external power source

$$\eta = \frac{E_{\text{st}}}{E_{\text{in}}} \tag{19}$$

where the stored energy E_{st} during the charging process is computed as [16]

$$E_{\text{st}} = \frac{1}{2}\sum_{k=1}^{n} C_k\left[v_0^2 - v_k^2(0)\right] \tag{20}$$

where $v_k(0)$ is the initial voltage of cell k, and the input energy E_{in} from the CC power source is derived as [18]

$$E_{\text{in}} = \sum_{k=1}^{n}\int_0^t v_k(\tau) i_c \mathrm{d}\tau = i_c \sum_{k=1}^{n}\int_0^t v_k(\tau)\mathrm{d}\tau \tag{21}$$

where t is the charging time for the supercapacitor energy system.

For different cases with the same reference voltage and initial voltages, the stored energy (20) during the charging process is the same. Thus, the energy efficiency is dominated by the input energy (21) from the CC power source. Since i_c is a constant, the input energy is determined by the area encircled by the voltage curve and charging time in the charging profile, as shown in (21). With the same charging time, the lower the voltage curve, the higher the energy efficiency will be. Following this observation, we will evaluate the energy efficiency of the proposed method under different communication topologies.

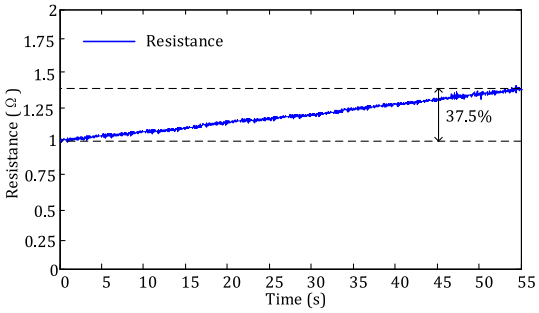

Fig. 4. Resistance deviation of a 1-Ω resistor with current $i_c = 5$ A.

3) Voltage Deviation: The voltage deviation during the charging process is an important metric to evaluate the performance of a cell-balancing system. The voltage deviation evaluates the maximal variation of cell voltages from the reference voltage when the charging process is completed. From Lemma 3, we know that cell voltages converge to the reference voltage $x_0 = i_c R$. However, in practical systems, the resistance R will have a gradual increase from the nominal value due to the thermal effect. Thus, cell voltages will continue increasing after they are fully charged. Fig. 4 shows the resistance deviation of a 1-Ω resistor with current $i_c = 5$ A. It is shown that the resistance increases by 37.5% after 55 s. Without a proper coordination among cells, the cells that first reach the reference voltage during the charging process will be overcharged.

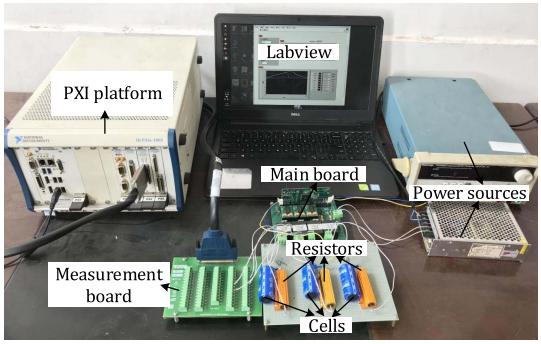

Fig. 5. Hardware setup of the supercapacitor energy storage system.

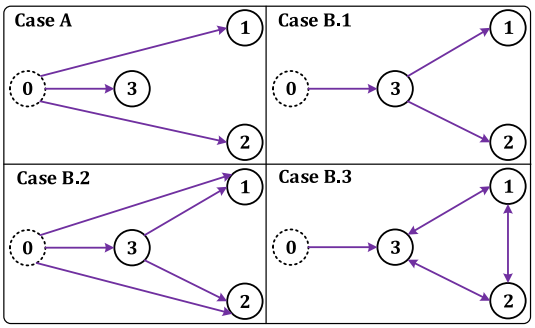

Fig. 6. Categorization of the communication topologies of three cells. Case A corresponds to the classical decentralized control method.

V. Performance Evaluation

In this section, we evaluate the performance of the proposed method with experimental results. We first introduce the hardware setup and parameter setting of the supercapacitor energy storage system. Then, experiments are conducted for each case. Some practical issues about the implementation of the proposed method are also discussed.

A. Hardware Setup

Fig. 5 shows the laboratory testbed of a three-cell supercapacitor energy storage system, which is built based on the schematic in Fig. 1. The main components of the testbed are introduced as follows.

1) *Main Board:* For compactness, several digital devices are embedded in the main board, including a TMS320F2808 microprocessor, three switches of type IRF530 MOSFET, three high-precision dividers working as voltage sensors, a PWM optocoupler/driver TLP700A, a low-pass filter chip TL074ID, and a voltage conversion chip PDUKE-24S05.
2) *Supercapacitor Cells:* Three Maxwell supercapacitor cells are connected in parallel with resistors through the corresponding IRF530 switches.
3) *Power Sources:* The CC power source supplies the charging current for the supercapacitor energy storage system. The DC 24 V power source supplies the operating voltage for the microcontrollers and sensors through the voltage conversion chip PDUKE-24S05.
4) *PXI Platform:* The PXI platform measures the voltages of the three cells through the measurement board and displays the voltage profiles with LabVIEW in the hosting computer. PXI is a rugged PC-based platform for measurement and automation systems, which has been proved as a high-performance and low-cost deployment platform for applications, such as manufacturing test, machine monitoring, automotive, and industrial test [38].

The operation mechanism of the testbed is described as follows. There are three control procedures (i.e., controllers) in the TMS320F2808 microprocessor. Each controller measures the voltage of the corresponding cell through the high-precision voltage divider. The measured analog voltage signals are filtered by the low-pass filter TL074ID. Three controllers transmit their local voltages to their neighbors based on the specified communication topology. With the filtered measurements and the voltage information transmitted from neighbors, each controller computes the duty cycles based on the control protocol (8)–(10). Then, the duty cycles are used to generate PWM signals to regulate the switches IRF530 MOSFETs through the PWM optocoupler/driver TLP700A. The TMS320F2808 microprocessor, which can provide 16 PWM outputs and 12-bit ADCs, has been programmed and debugged with the Code Composer Studio (CCS) in the hosting computer. The switching frequency $f_s = 10$ kHz.

B. Parameter Setting

The physical-layer parameters are given first, and then different cyber model parameters are considered in the performance evaluation.

1) Physical Setting: We consider the three cells in the supercapacitor energy storage system shown in Fig. 1, where the circuit parameters are given as follows: the nominal capacitances of three cells $C_1 = C_2 = C_3 = 130$ F, charging current $i_c = 2$ A, reference voltage $v_0 = 2$ V, and balancing resistance $R = 1\ \Omega$. The voltage imbalance typically occurs due to the manufacturing tolerance. To emulate the phenomena, the initial voltages of the three cells are set differently as $v_1(0) = 1.2$ V, $v_2(0) = 0.9$ V, and $v_3(0) = 0.6$ V.

2) Cyber Setting: Without loss of generality, we consider four cases of communication topologies in the performance evaluation. The categorization of the communication topologies is depicted in Fig. 6, which is described as follows.

a) Case A: In this case, the reference pins to each cell and there are no interactions among cells. This case corresponds to the classical decentralized control method in the literature. The communication topology is characterized mathematically by

$$\mathbf{G} = \begin{bmatrix} 1 & 0 & 0 \\ 0 & 1 & 0 \\ 0 & 0 & 1 \end{bmatrix}, \quad \mathbf{L} = \begin{bmatrix} 0 & 0 & 0 \\ 0 & 0 & 0 \\ 0 & 0 & 0 \end{bmatrix}.$$

b) Case B.1: In this case, the reference pins to cell 3, and cell 3 acts as the root for a minimum spanning tree among cells, i.e., cells interact with the reference and with each

other through a minimal number of links. The communication topology is characterized mathematically by

$$\mathbf{G} = \begin{bmatrix} 0 & 0 & 0 \\ 0 & 0 & 0 \\ 0 & 0 & 1 \end{bmatrix}, \quad \mathbf{L} = \begin{bmatrix} 1 & 0 & -1 \\ 0 & 1 & -1 \\ 0 & 0 & 0 \end{bmatrix}.$$

c) Case B.2: In this case, the reference pins to three cells and cell 3 is the root of the minimum spanning tree among cells, i.e., cells interact with each other through the minimum spanning tree links, but interact with the reference through the redundant and direct links. The communication topology is characterized mathematically by

$$\mathbf{G} = \begin{bmatrix} 1 & 0 & 0 \\ 0 & 1 & 0 \\ 0 & 0 & 1 \end{bmatrix}, \quad \mathbf{L} = \begin{bmatrix} 1 & 0 & -1 \\ 0 & 1 & -1 \\ 0 & 0 & 0 \end{bmatrix}.$$

d) Case B.3: In this case, the reference pins to cell 3, and there is an undirected ring topology among the three cells, i.e., cells interact with the reference through a minimal number of links, but interact with each other through the redundant links. The communication topology is characterized mathematically by

$$\mathbf{G} = \begin{bmatrix} 0 & 0 & 0 \\ 0 & 0 & 0 \\ 0 & 0 & 1 \end{bmatrix}, \quad \mathbf{L} = \begin{bmatrix} 2 & -1 & -1 \\ -1 & 2 & -1 \\ -1 & -1 & 2 \end{bmatrix}.$$

Another trivial case is that cells interact with the reference and with each other both through the redundant links. The effect of this case can be evaluated by analyzing Cases B.2 and B.3 together, and thus omitted here.

C. Experiment Results

The experiment results for Cases A–B.3 are provided in Figs. 7–10, respectively. The analysis of the experiment results is summarized in what follows.

1) Case A: In Case A, cells compute their duty cycles (0/1) by comparing their local voltages with the reference independently. Fig. 7 shows the experiment results of Case A. The charging profiles of the three cells are shown in Fig. 7(a), where the three cells are charged independently of their initial voltages to the reference voltage. The charging time of the energy storage system is $T = 94$ s, which is dominated by cell 3. Based on the energy efficiency (19) and charging profiles in Fig. 7(a), we compute the energy efficiency as 73.5%. The switching signals for the three cells are shown in Fig. 7(b). We can find that the switching signals are 1 before the corresponding cells are fully charged, i.e., cells work in the fast-charging mode, while when the cells are fully charged, the switching signals are switched from 1 to 2, i.e., cell voltages are expected to be stabilized at the desired value. Note that when the tracking error δ_k $(k = 1, 2, 3)$ approaches zero, the switching signal σ_k has a frequent switching due to the measurement noise. However, cell voltages $i_c R$ are soon larger than the desired voltage v_0 due to the thermal effect of balancing resistors, i.e., the tracking error will be less than zero, and then the switching signals will be maintained at 2 based on (9). The voltage deviation effects of Case A are shown in Fig. 7(c), from which we find that when cells 1 and 2 are fully

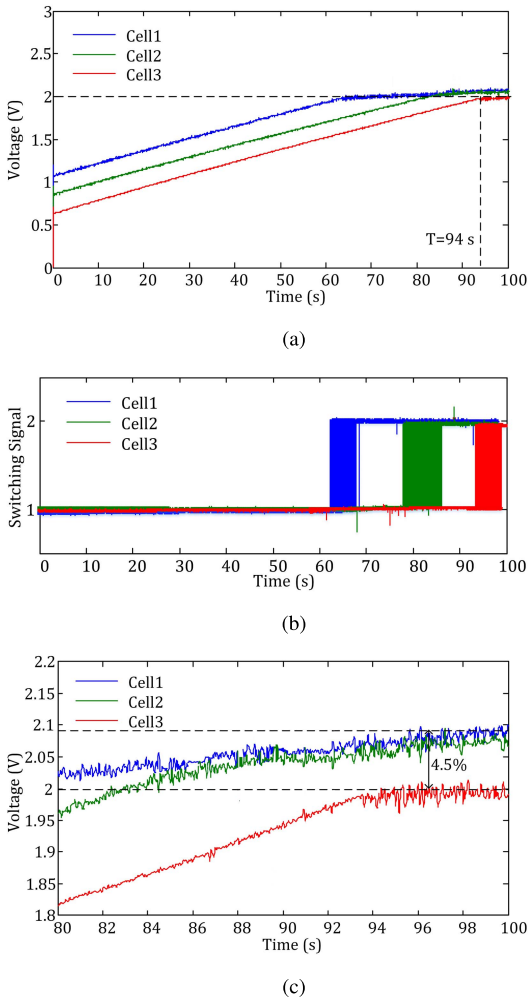

Fig. 7. Experimental results of Case A (the classical decentralized control method). (a) Charging profile. (b) Switching signal. (c) Voltage deviation.

charged, their voltages continue increasing until the charging is terminated. This is because the resistance of balancing resistors is larger than the nominal value $R = 1\ \Omega$ due to the thermal heating during the charging process. Then, from Lemma 3, we know that the final voltage $i_c R$ of cells 1 and 2 will be above the nominal value $v_0 = 2$ V, i.e., cells are overcharged. As shown in Fig. 7(c), the maximal voltage deviation of Case A is 4.5%.

2) Case B.1: In Case B.1, cell 3 computes its duty cycle by comparing its voltage with the reference, while cells 1 and 2 compute their duty cycles by comparing their voltages with that of cell 3. Fig. 8 shows the experimental results of Case B.1. The charging profiles of the three cells are shown in Fig. 8(a), where cell 3 is charged independently, and cells 1 and 2 are charged by following cell 3. Three cells are synchronized around 60 s. The charging time of the energy storage system is $T = 94$ s, which is the same as Case A since the charging time is still dominated by cell 3. The energy efficiency of Case B.1 is computed as 81%, which is higher than that of Case A. This is because the voltages of cells 1 and 2 keep low profiles by tracking cell 3 instead of the reference. The switching signals for the three cells are

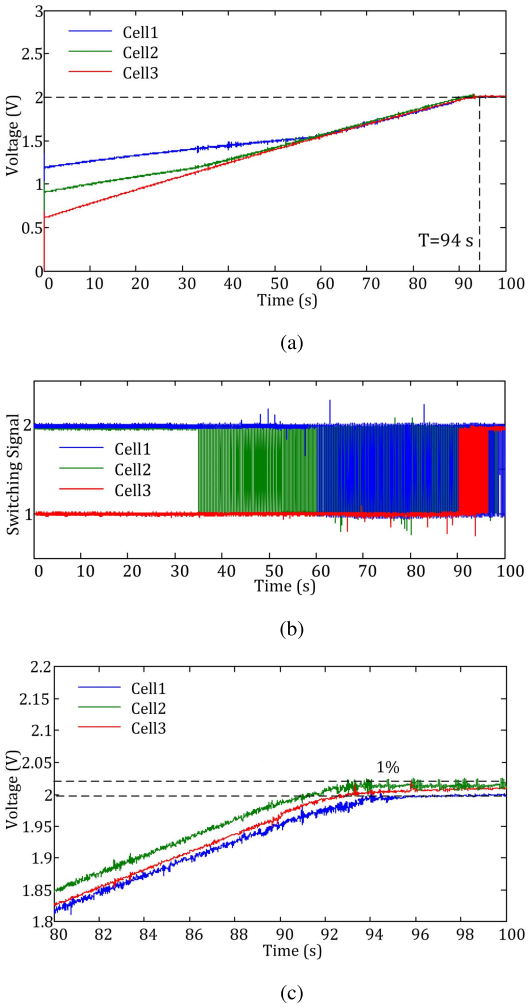

Fig. 8. Experiment results of Case B.1. (a) Charging profile. (b) Switching signal. (c) Voltage deviation.

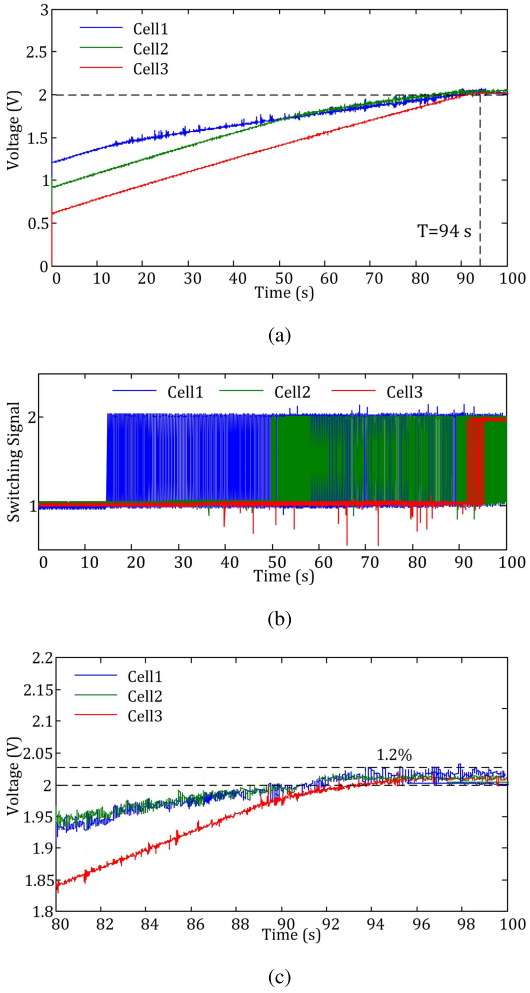

Fig. 9. Experiment results of Case B.2. (a) Charging profile. (b) Switching signal. (c) Voltage deviation.

shown in Fig. 8(b). The switching signal of cell 3 is the same as that of Case A, as cell 3 is still charged independently. Cell 1's switching signal is 2 before 60 s, as the tracking error $\delta_1 = v_3 - v_1$ is negative from 0 to 60 s. When the tracking error δ_1 approaches and maintains at zero after 60 s, there are frequent switchings due to the measurement noise. The switching signal for cell 2 can be analyzed similarly. The voltage deviation effects of Case B.1 are shown in Fig. 8(c), where the maximal voltage deviation is about 1%, which is far less than Case A. This is because the interactions among cells alleviate the voltage deviation effect through the voltage synchronization during the charging process.

3) Case B.2: In Case B.2, cell 3 computes its duty cycle by comparing its voltage with the reference, while cells 1 and 2 compute their duty cycles by comparing their voltages with both the reference and cell 3's voltage. The experimental results of Case B.2 are shown in Fig. 9. The charging profiles of the three cells are shown in Fig. 9(a), where cell 3 is charged independently, and cells 1 and 2 are charged by following both the reference and cell 3. The charging time of the energy storage system is $T = 94$ s, and cells are synchronized when the charging process is completed at 94 s. The energy efficiency of Case B.2 is computed as 77%, which is higher than Case A but lower than Case B.1. This can be explained by the charging profiles of cells 1 and 2, where these profiles of Case B.2 are higher than those of Case B.1 but lower than those of Case A. The switching signals for the three cells are shown in Fig. 9(b). Cell 3's switching signal is still 1 before 94 s and becomes 2 afterward. The switching signals of cells 1 and 2 are 1 before 15 and 50 s, respectively, as the corresponding tracking errors δ_1 and δ_2 are positive. When δ_1 and δ_2 approach and maintain at zero after 15 and 50 s, respectively, the switching signals have frequent switchings similarly. The voltage deviation effects are shown in Fig. 9(c), where the maximal voltage deviation is 1.2%.

4) Case B.3: In Case B.3, cell 3 computes its duty cycle by comparing its voltage with both the reference and the voltages of the other two cells, while cells 1 and 2 compute their duty cycles by comparing their voltages with those of the other two cells, respectively. Fig. 10 shows the experimental results of Case B.3. The charging profiles of the three cells are shown in Fig. 10(a), where cell 3 is charged by tracking both the reference and the voltages of cells 1 and 2, while

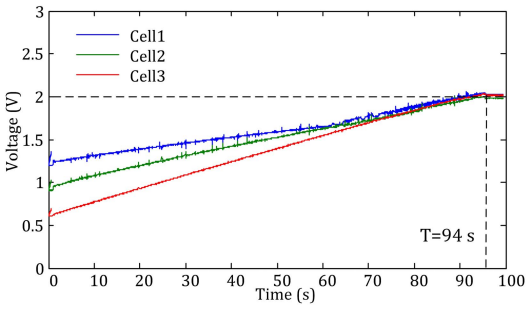

(a)

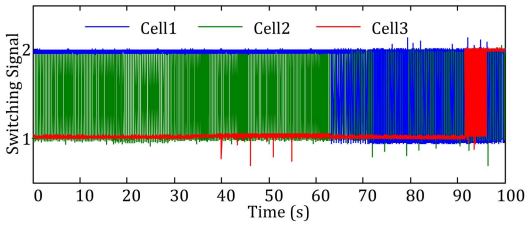

(b)

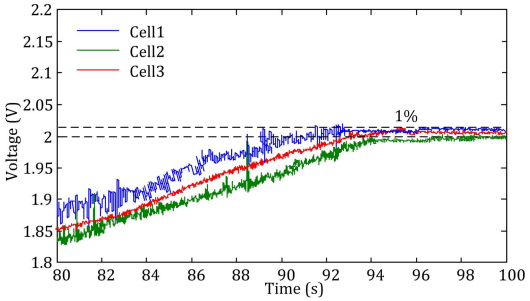

(c)

Fig. 10. Experiment results of Case B.3. (a) Charging profile. (b) Switching signal. (c) Voltage deviation.

cells 1 and 2 are charged by tracking the voltages of the other two cells, respectively. The charging time of the energy storage system is $T = 94$ s, which is still dominated by cell 3. This is because the voltage feedback from cells 1 and 2 to cell 3 is always positive before they are fully charged. Then, from (9), we know that cell 3 is still charged by $s_3 = 0$ during the charging process. The energy efficiency of Case B.3 is computed as 79.3%. The switching signals of the three cells are shown in Fig. 10(b). The switching signal of cell 3 is the same as those of Figs. 7–9. Cell 1's switching signal is 2 before 65 s, as the tracking error δ_1 is negative and switches frequently when the tracking error δ_1 approaches zero after 65 s. Note that cell 2's switching signal switches rapidly to synchronize its voltage with those of cells 1 and 3 from 0 s. The voltage deviation effects of Case B.3 are shown in Fig. 10(c), where the maximal voltage deviation is 1%.

D. Results and Discussion

The performance metrics of the proposed method under different communication topologies are summarized in Table I, where the charging time, energy efficiency, and voltage deviation are considered. The experimental results are discussed as follows.

TABLE I
SUMMARY OF THE PERFORMANCE EVALUATION

Metric\Case No.	A	B.1	B.2	B.3
Charging Time (s)	94	94	94	94
Energy Efficiency	73.5%	81%	77%	79.3%
Voltage Deviation	4.5%	1%	1.2%	1%

1) Charging Time: In Case A and Cases B.1–B.3, the charging time is always dominated by cell 3. This is because cell 3 is chosen as the pinned root in the graph. In these cases, cell 3 is charged with duty cycle $s_3 = 0$ before it is fully charged since the tracking errors are always positive. Thus, all these cases have the same charging time.

It is worth noting that the charging time may be prolonged by the cell-balancing system. For comparison, we consider the leaderless consensus protocols [27]–[29], where the communication topology is

$$\mathbf{G} = \begin{bmatrix} 0 & 0 & 0 \\ 0 & 0 & 0 \\ 0 & 0 & 0 \end{bmatrix}, \quad \mathbf{L} = \begin{bmatrix} 2 & -1 & -1 \\ -1 & 2 & -1 \\ -1 & -1 & 2 \end{bmatrix}.$$

Note that the Laplacian matrix is the same as that of Case B.3, and the only difference is that the pinning matrix is a zero matrix in the leaderless consensus protocols. Experimental results of the leaderless consensus-based cell-balancing method are shown in Fig. 11. By comparing Fig. 10(a) with Fig. 11(a), we find that the charging time of three cells is prolonged from 94 to 120 s. This can be explained by examining the switching signals of cell 3 in Figs. 10(b) and 11(b). In Fig. 10(b), cell 3 is always charged with switching signal 1 (i.e., fast charging mode) before cells are fully charged at 94 s. However, in Fig. 11(b), we can see that the switching signal of cell 3 has a frequent switching between 1 and 2 to synchronize its voltage with the other two cells from 50 s, which significantly prolongs the charging time. This fact implies that the pinner is useful in shortening the charging time.

2) Energy Efficiency: As explained previously, the energy efficiency is dominated by the charging profiles of the three cells. Since cell 3 has the same charging profile in all four cases, the energy efficiency of the system is determined by the profiles of cells 1 and 2. Case B.1 has the highest energy efficiency because cells 1 and 2 keep low profiles by tracking cell 3 instead of the reference voltage. Case A has the lowest energy efficiency, as cells 1 and 2 maintain high profiles by tracking the reference directly. The energy efficiency of Case B.2 is slightly lower than that of Case B.3 because cells 1 and 2 in Case B.2 have relatively high profiles by tracking both the reference and cell 3.

3) Voltage Deviation: From Table I, we find that Case A has the largest voltage deviation, while Cases B.1–B.3 have relatively small voltage deviations. This is because in Case A, when cells 1 and 2 are fully charged, they have to shunt the charging current to resistors to wait for cell 3 to be fully

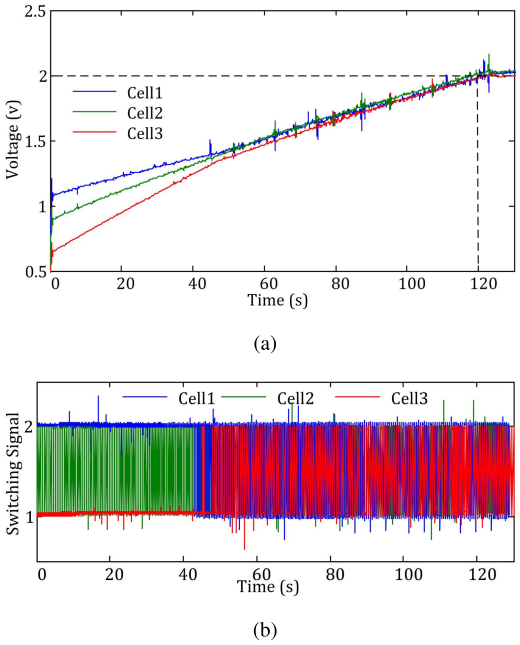

Fig. 11. Experimental results of the leaderless consensus-based cell-balancing method. (a) Charging profile. (b) Switching signal.

charged. However, due to the thermal effect, the balancing resistance will increase gradually and the charging current cannot be totally shunted to the balancing resistors. Thus, cells 1 and 2 are overcharged during the shunting stage. In Cases B.1–B.3, cells are synchronized during the charging process and reach the reference voltage synchronously. Thus, the shunting stage is avoided and the voltage deviation is alleviated.

E. Practical Issues

We further discuss some practical issues about the implementation of the proposed method: 1) the benefits and the associated costs of the proposed method; 2) how to choose the pinned node in the implementation; and 3) how to extend the proposed method to the discharging case.

1) Superiority: Experimental results show that the proposed method can effectively improve the energy efficiency and reduce the voltage deviation compared with the existing decentralized control method. The higher energy efficiency means less power loss consumed in balancing resistors, implying that the charging system is greener and the thermal heating of resistors can be alleviated. The reduced voltage deviation protects cells from overcharging, which prolongs the lifetime of supercapacitors and improves the reliability of the energy storage system.

2) Hardware Cost: The communications among cells do not necessarily introduce additional hardware cost. In small-scale energy storage systems, where a single microcontroller can provide enough hardware resources (e.g., IO ports), all cells can be connected to a single microcontroller. Then, we can design distributed control procedures (controllers) for each cell in the microcontroller, where the communications among cells are realized with the signal flows in the software design, calling for no additional hardware cost. In this paper, three cells are directly connected to the TMS320F2808 microprocessor without communication hardware costs.

3) Scalability: In large-scale energy storage systems where geographically distributed microcontrollers are deployed, additional communication hardware resources are required for the voltage synchronization of cells in the charging process. However, the pinning control strategy is a distributed control method, i.e., cells only communicate with their neighbors to make a control decision. This implies that only a sparse communication network is required and the proposed method benefits from a good scalability, i.e., the complexity of the design will not increase with the number of cells. Thus, the proposed method is applicable to large-scale energy storage systems.

4) Pinned Node: From the experimental results, we find that Case B.1 has the highest energy efficiency in the case study. This is because, in the other cases, the redundant communication links from the reference to the pinned nodes or the redundant links among the nodes result in high charging profiles of cells, which reduce the energy efficiency of the charging system. In Case B.1, there is only one pinned node (i.e., cell 3) and the pinned node interacts with the other cells (i.e., cells 1 and 2) through a minimum spanning tree. The minimal number of communication links achieves the voltage synchronization as well as improves the energy efficiency during the charging process. Since low charging profiles lead to high energy efficiency, we typically choose the cell with the lowest charging profile as the pinned node. Then, the energy efficiency of the charging system can be improved if the voltages of the other cells are synchronized with the pinned node. In this paper, we choose cell 3 as the pinned node as it has the lowest charging profiles.

5) Discharging: In the charging of cells, the objective of the cell balancing is to prevent cells from overcharging. In the discharging of cells, however, the primary task is to prevent cells from overdischarging. For the switched resistor circuit, a straightforward discharging approach is to discharge cells with all switches OFF and monitor the cell with the lowest voltage. When the voltage is lower than the safety threshold, the discharging process can be terminated to prevent the cell from overdischarging.

The proposed method can be extended to the discharging case. For instance, we consider that the initial voltages of three cells are $v_1(0) = 2$ V, $v_2(0) = 1.9$ V, and $v_3(0) = 1.8$ V, and the communication topology as

$$\mathbf{G} = \begin{bmatrix} 0 & 0 & 0 \\ 0 & 0 & 0 \\ 0 & 0 & 0 \end{bmatrix}, \quad \mathbf{L} = \begin{bmatrix} 1 & 0 & -1 \\ 0 & 1 & -1 \\ 0 & 0 & 0 \end{bmatrix}.$$

The discharging profiles of three cells are shown in Figs. 12 and 13, where the three cells are discharging through a common 4-Ω load. Fig. 12 shows the experimental results of three cells with all switches OFF, i.e., cells are discharged independently. As shown in Fig. 12(a), when the cell with the lowest voltage (i.e., cell 3) reaches the safety threshold (e.g., 1.2 V), the discharging is terminated to prevent any

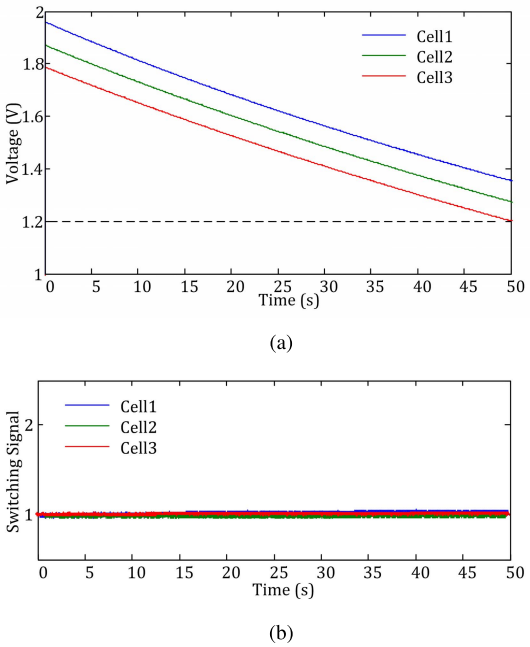

Fig. 12. Discharging of three cells with all switches OFF. (a) Discharging profile. (b) Switching signal.

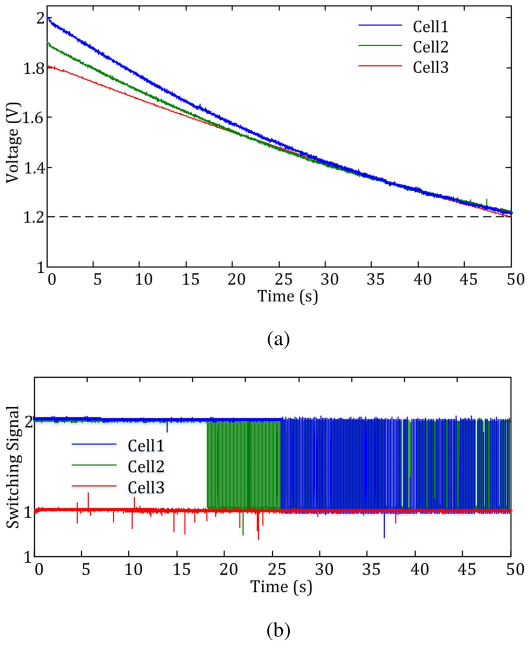

Fig. 13. Discharging of three cells with the proposed method. (a) Discharging profile. (b) Switching signal.

cells from overdischarging. Fig. 12(b) shows that the switching signals of three cells are all 1, i.e., cells are discharged with switches OFF. Fig. 13 shows the experimental results of the proposed method. As shown in Fig. 13(a), cell voltages are synchronized during the discharging process and reach the safety threshold (e.g., 1.2 V) simultaneously. Fig. 13(b) shows the switching signals of three cells, where cell 3's switching signal is always 1, while the switching signals of cells 1 and 2 are 2 before 26 and 17 s, and then they switch frequently to synchronize cell voltages after 26 and 17 s, respectively.

It is worth noting that, although the voltage synchronization improves the energy efficiency during the charging process, it is not necessarily true for the discharging process. This is because, as long as the switches are turned on during the discharging process, there will be additional energy consumptions on balancing resistors. Thus, the most energy-efficient discharging method is to discharge cells with all switches OFF, but it may cause some balancing concerns.

VI. Conclusion

In this paper, we proposed a pinning-based switching control method for supercapacitor energy storage systems. The stability and convergence of the closed-loop system have been proved rigorously. The performance of the proposed method is analyzed in the unified framework and is further verified with extensive experimental results. It is shown that the classical decentralized control method is a special case of the proposed design. Moreover, the performance metrics of the energy storage system, including voltage deviation and energy efficiency, have been improved considerably.

Future works focus on two main aspects: 1) exploring the analytical relationship between the communication topology and balancing time and 2) developing advanced control laws to reduce the chattering phenomenon of switches.

References

[1] J. P. Torreglosa, P. García, L. M. Fernández, and F. Jurado, "Predictive control for the energy management of a fuel-cell–battery–supercapacitor tramway," *IEEE Trans. Ind. Informat.*, vol. 10, no. 1, pp. 276–285, Feb. 2014.

[2] Y. Zhang, Z. Wei, H. Li, L. Cai, and J. Pan, "Optimal charging scheduling for catenary-free trams in public transportation systems," *IEEE Trans. Smart Grid*, vol. 10, no. 1, pp. 227–237, Jan. 2018.

[3] H. Li, J. Peng, W. Liu, and Z. Huang, "Stationary charging station design for sustainable urban rail systems: A case study at Zhuzhou electric locomotive Co., China," *Sustainability*, vol. 7, no. 1, pp. 465–481, Jan. 2015.

[4] L. Sun, K. Feng, C. Chapman, and N. Zhang, "An adaptive power-split strategy for battery–supercapacitor powertrain—Design, simulation, and experiment," *IEEE Trans. Power Electron.*, vol. 32, no. 12, pp. 9364–9375, Dec. 2017.

[5] D. B. W. Abeywardana, B. Hredzak, V. G. Agelidis, and G. D. Demetriades, "Supercapacitor sizing method for energy-controlled filter-based hybrid energy storage systems," *IEEE Trans. Power Electron.*, vol. 32, no. 2, pp. 1626–1637, Feb. 2017.

[6] D. B. W. Abeywardana, B. Hredzak, and V. G. Agelidis, "A fixed-frequency sliding mode controller for a boost-inverter-based battery-supercapacitor hybrid energy storage system," *IEEE Trans. Power Electron.*, vol. 32, no. 1, pp. 668–680, Jan. 2017.

[7] N. A. Kyeremateng, T. Brousse, and D. Pech, "Microsupercapacitors as miniaturized energy-storage components for on-chip electronics," *Nature Nanotechnol.*, vol. 12, no. 1, pp. 7–15, Nov. 2016.

[8] F. Deng, H. Qiu, J. Chen, L. Wang, and B. Wang, "Wearable thermoelectric power generators combined with flexible supercapacitor for low-power human diagnosis devices," *IEEE Trans. Ind. Electron.*, vol. 64, no. 2, pp. 1477–1485, Feb. 2017.

[9] Y. Song, X.-X. Chen, J.-X. Zhang, X.-L. Cheng, and H.-X. Zhang, "Freestanding micro-supercapacitor with interdigital electrodes for low-power electronic systems," *J. Microelectromech. Syst.*, vol. 26, no. 5, pp. 1055–1062, Oct. 2017.

[10] R. Drummond, S. Zhao, and S. R. Duncan, "Design tools for electrochemical supercapacitors using local absolute stability theory," *IEEE Trans. Control Syst. Technol.*, vol. 27, no. 3, pp. 1071–1083, May 2019.

[11] L. Zhang, X. Hu, Z. Wang, F. Sun, and D. Dorrell, "A review of supercapacitor modeling, estimation, and applications: A control/management perspective," *Renew. Sustain. Energy Rev.*, vol. 81, no. 2, pp. 1868–1878, Jan. 2018.

[12] Y. Parvini, A. Vahidi, and S. A. Fayazi, "Heuristic versus optimal charging of supercapacitors, lithium-ion, and lead-acid batteries: An efficiency point of view," *IEEE Trans. Control. Syst. Technol.*, vol. 26, no. 1, pp. 167–180, Jan. 2018.

[13] H. Chaoui, A. El Mejdoubi, A. Oukaour, and H. Gualous, "Online system identification for lifetime diagnostic of supercapacitors with guaranteed stability," *IEEE Trans. Control Syst. Technol.*, vol. 24, no. 6, pp. 2094–2102, Nov. 2016.

[14] D. Linzen, S. Buller, E. Karden, and R. W. De Doncker, "Analysis and evaluation of charge-balancing circuits on performance, reliability, and lifetime of supercapacitor systems," *IEEE Trans. Ind. Appl.*, vol. 41, no. 5, pp. 1135–1141, Sep./Oct. 2005.

[15] K. Maneesut and U. Supatti, "Reviews of supercapacitor cell voltage equalizer topologies for EVs," in *Proc. 14th Int. Conf. Elect. Eng./Electron., Comput., Telecommun. Inf. Technol. (ECTI-CON)*, Jun. 2017, pp. 608–611.

[16] F. M. Ibanez, "Analyzing the need for a balancing system in supercapacitor energy storage systems," *IEEE Trans. Power Electron.*, vol. 33, no. 3, pp. 2162–2171, Mar. 2018.

[17] S. Shili, A. Hijazi, A. Sari, X. Lin-Shi, and P. Venet, "Balancing circuit new control for supercapacitor storage system lifetime maximization," *IEEE Trans. Power Electron.*, vol. 32, no. 6, pp. 4939–4948, Jun. 2017.

[18] H. Li *et al.*, "SoH-aware charging of supercapacitors with energy efficiency maximization," *IEEE Trans. Energy Convers.*, vol. 33, no. 4, pp. 1766–1775, Dec. 2018.

[19] X. Li, X. Wang, and G. Chen, "Pinning a complex dynamical network to its equilibrium," *IEEE Trans. Circuits Syst. I, Reg. Papers*, vol. 51, no. 10, pp. 2074–2087, Oct. 2004.

[20] Y. Lu and W. Zhang, "On switching stabilizability for continuous-time switched linear systems," *IEEE Trans. Autom. Control*, vol. 61, no. 11, pp. 3515–3520, Nov. 2016.

[21] W. Xiang, H.-D. Tran, and T. T. Johnson, "Output reachable set estimation for switched linear systems and its application in safety verification," *IEEE Trans. Autom. Control*, vol. 62, no. 10, pp. 5380–5387, Oct. 2017.

[22] Y. Lu and W. Zhang, "A piecewise smooth control-Lyapunov function framework for switching stabilization," *Automatica*, vol. 76, pp. 258–265, Feb. 2017.

[23] Z. Meng, W. Ren, Y. Cao, and Z. You, "Leaderless and leader-following consensus with communication and input delays under a directed network topology," *IEEE Trans. Syst., Man, Cybern. B. Cybern.*, vol. 41, no. 1, pp. 75–88, Feb. 2011.

[24] S. Manaffam, M. K. Talebi, A. K. Jain, and A. Behal, "Synchronization in networks of identical systems via pinning: Application to distributed secondary control of microgrids," *IEEE Trans. Control Syst. Technol.*, vol. 25, no. 6, pp. 2227–2234, Nov. 2017.

[25] C. Yan, H. Fang, and H. Chao, "Energy-aware leader-follower tracking control for electric-powered multi-agent systems," *Control Eng. Pract.*, vol. 79, pp. 209–218, Oct. 2018.

[26] H. Li, J. Peng, J. He, R. Zhou, Z. Huang, and J. Pan, "A cooperative charging protocol for onboard supercapacitors of catenary-free trams," *IEEE Trans. Control Syst. Technol.*, vol. 26, no. 4, pp. 1219–1232, Jul. 2018.

[27] Q. Ouyang, J. Chen, J. Zheng, and H. Fang, "Optimal cell-to-cell balancing topology design for serially connected Lithium-Ion battery packs," *IEEE Trans. Sustain. Energy*, vol. 9, no. 1, pp. 350–360, Jan. 2018.

[28] H. Li, J. Peng, J. He, Z. Huang, and J. Pan, "Synchronized cell-balancing charging of supercapacitors," *IFAC-PapersOnLine*, vol. 50, no. 1, pp. 3338–3343, Jul. 2017.

[29] L. Y. Wang, F. Lin, and W. Chen, "Controllability, observability, and integrated state estimation and control of networked battery systems," *IEEE Trans. Control Syst. Technol.*, vol. 26, no. 5, pp. 1699–1710, Sep. 2018.

[30] R. A. DeCarlo, M. S. Branicky, S. Pettersson, and B. Lennartson, "Perspectives and results on the stability and stabilizability of hybrid systems," *Proc. IEEE*, vol. 88, no. 7, pp. 1069–1082, Jul. 2000.

[31] D. Liberzon and A. S. Morse, "Basic problems in stability and design of switched systems," *IEEE Control Syst.*, vol. 19, no. 5, pp. 59–70, Oct. 1999.

[32] Z. Sun and S. S. Ge, "Analysis and synthesis of switched linear control systems," *Automatica*, vol. 41, no. 2, pp. 181–195, 2005.

[33] M. Wicks, P. Peleties, and R. DeCarlo, "Switched controller synthesis for the quadratic stabilisation of a pair of unstable linear systems," *Eur. J. Control*, vol. 4, no. 2, pp. 140–147, 1998.

[34] M. A. Wicks, P. Peleties, and R. A. DeCarlo, "Construction of piecewise Lyapunov functions for stabilizing switched systems," in *Proc. 33rd IEEE Conf. Decis. Control*, vol. 4, Dec. 1994, pp. 3492–3497.

[35] E. Feron, *Quadratic Stabilizability of Switched Systems via State and Output Feedback*. Atlanta, GA, USA: Center for Intelligent Control Systems, 1996.

[36] D. B. West *et al.*, *Introduction to Graph Theory*, vol. 2. Upper Saddle River, NJ, USA: Prentice-Hall, 2001.

[37] A. W. Colombo, S. Karnouskos, O. Kaynak, Y. Shi, and S. Yin, "Industrial cyberphysical systems: A backbone of the fourth industrial revolution," *IEEE Ind. Electron. Mag.*, vol. 11, no. 1, pp. 6–16, Mar. 2017.

[38] *What is PXI?* Accessed: Jun. 1, 2018. [Online]. Available: http://www.ni.com/pxi/whatis/

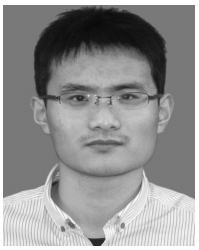

Heng Li (M'17) received the bachelor's and Ph.D. degrees from Central South University, Changsha, China, in 2011 and 2017, respectively.

From 2015 to 2017, he was a Research Assistant with the Department of Computer Science, University of Victoria, Victoria, BC, Canada. He is currently an Assistant Professor with the School of Computer Science and Engineering, Central South University. His current research interests include cooperative control and energy storage systems.

Jun Peng (M'08) received the B.S. degree from Xiangtan University, Xiangtan, China, in 1987, the M.Sc. degree from the National University of Defense Technology, Changsha, China, in 1990, and the Ph.D. degree from Central South University, Changsha, in 2005.

In 1990, she joined the Staff of Central South University, where she is currently a Professor with the School of Computer Science and Engineering. From 2006 to 2007, she was with the School of Electrical and Computer Science, University of Central Florida, Orlando, FL, USA, as a Visiting Scholar. Her current research interests include cooperative control, cloud computing, and wireless communications.

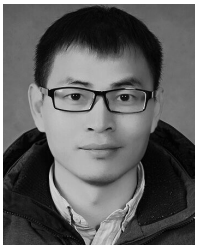

Jianping He (M'15) received the Ph.D. degree in control science and engineering from Zhejiang University, Hangzhou, China, in 2013.

He had been a Research Fellow with the Department of Electrical and Computer Engineering, University of Victoria, Victoria, BC, Canada, from 2013 to 2017. He is currently an Associate Professor with the Department of Automation, Shanghai Jiao Tong University, Shanghai, China. His current research interests include smart sensing and control, security and privacy theory and applications, distributed learning, and big data.

Dr. He received the Best Paper Award of the IEEE WCSP 2017 and the finalist Best Student Paper Award of the IEEE ICCA 2017. He serves as an Associate Editor for the *KSII Transactions on Internet and Information Systems*. He was also a Guest Editor of the *International Journal of Robust and Nonlinear Control* and *Neurocomputing*.

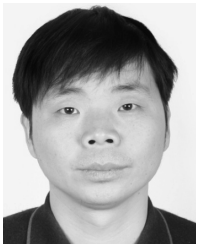

Zhiwu Huang (M'08) received the B.S. degree in industrial automation from Xiangtan University, Xiangtan, China, in 1987, the M.S. degree in industrial automation from the Department of Automatic Control, University of Science and Technology Beijing, Beijing, China, in 1989, and the Ph.D. degree in control theory and control engineering from Central South University, Changsha, China, in 2006.

In 1994, he joined the Staff of Central South University, where is currently a Professor with the School of Automation. From 2008 to 2009, he was with the School of Computer Science and Electronic Engineering, University of Essex, Colchester, U.K., as a Visiting Scholar. His research interests include fault diagnostic technique and cooperative control.

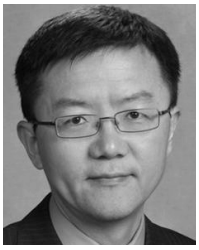

Jing Wang (M'00–SM'11) received the Ph.D. degree in control theory and control engineering from Central South University, Changsha, China, in 1997.

He was a Post-Doctoral Research Fellow with the Institute of Computing Technology, Chinese Academy of Sciences, Beijing, China, from 1997 to 1999, and with the Department of Electrical and Computer Engineering, National University of Singapore, Singapore, from 1999 to 2002. From 2002 to 2007, he was with the School of Electrical Engineering and Computer Science, University of Central Florida, Orlando, FL, USA, as a Research Assistant Professor. From 2007 to 2014, he was with the Department of Computer Engineering, Bethune Cookman University, Daytona Beach, FL, USA, first as an Assistant Professor and then as a tenured Associate Professor. Since 2014, he has been with the Department of Electrical and Computer Engineering, Bradley University, Peoria, IL, USA. His current research interests include systems and controls, distributed optimization and machine learning, robotics, and control applications.

Liang He (S'09–M'12–SM'17) was a Research Scientist with the University of Victoria, Victoria, BC, Canada, from 2009 to 2011, and with the Singapore University of Technology and Design, Singapore, from 2012 to 2014, and a Research Fellow with the University of Michigan, Ann Arbor, MI, USA, from 2015 to 2017. He is currently an Assistant Professor with the University of Colorado Denver, Denver, CO, USA. His current research interests include CPSes, cognitive battery management, and networking.

Dr. He has been a recipient of the best paper/poster awards of MobiSys 2017, QShine 2014, WCSP 2011, and GLOBECOM 2011, and the best paper candidate of GLOBECOM 2014.

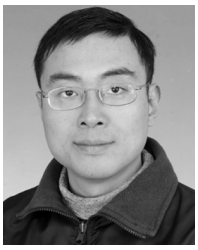

Jianping Pan (S'96–M'98–SM'08) received the bachelor's and Ph.D. degrees in computer science from Southeast University, Nanjing, China.

He did his post-doctoral research at the University of Waterloo, Waterloo, ON, Canada. He was also with Fujitsu Labs, San Francisco, CA, USA, and NTT Labs. His area of specialization is computer networks and distributed systems. He is currently a Professor of computer science with the University of Victoria, Victoria, BC, Canada. His current research interests include protocols for advanced networking, performance analysis of networked systems, and applied network security.

Dr. Pan is a Senior Member of the ACM. He received the IEICE Best Paper Award in 2009, the Telecommunications Advancement Foundations' Telesys Award in 2010, the WCSP 2011 Best Paper Award, the IEEE Globecom 2011 Best Paper Award, the JSPS Invitation Fellowship in 2012, and the IEEE ICC 2013 Best Paper Award.